SSRG International Journal of Electrical and Electronics Engineering
ISSN: 2348-8379/ https://doi.org/10.14445/23488379/IJEEE-V10I11P109
Volume 10 Issue 11 89-99, November 2023

Original Article

Enhanced the Performance of Solar Photovoltaic (PV) Power Systems Based on ANFIS-MPPT P&O Using A Boost Converter

Nguyen Van Bao[1,2], Chu Thi Thuy[1], Vo Quang Vinh[3], Vo Thanh Ha[4]

[1]*Department of Control and Automation, University of Economics-Technology for Industries, Hanoi, Vietnam.*
[2]*Vietnam Russia Vocational Training College No. 1,Vinh Phuc, Vietnam.*
[3]*Department of Control Engineering, University of Electricity, Hanoi, Vietnam.*
[4]*Department of Cybernetics, University of Transport and Communications, Hanoi, Vietnam.*

[4]*Corresponding Author : vothanhha.ktd@utc.edu.vn*

Received: 20 September 2023 Revised: 23 October 2023 Accepted: 18 November 2023 Published: 02 December 2023

Abstract *- This paper introduces the MPPT control method to help PV solar cells reach the maximum capacity thanks to the adaptive ANFIS P&O MPPT algorithm. The power from the PV source through the traditional PI-controlled boost converter has a working point that always follows the MPPT point. Thanks to the ANFIS P&O MPPT algorithm that allows adaptive correction of the perturbation step, the power can quickly reach a new maximum value when the ambient temperature and illuminance fluctuate. The new algorithm also eliminates oscillation around the MPPT's entire operating point and improves the output voltage quality of the boost converter. The advantage of the adaptive ANFIS P&O MPPT algorithm is confirmed by simulation on MATLAB with a 3.5kW, 100V of the PV system. According to simulation findings, the suggested ANFIS-based MPPT can consistently and efficiently monitor the maximum power point of PV modules under various weather circumstances.*

Keywords *- PV, MPPT P&O, ANFIS, Boost converter, Solar power system.*

1. Introduction

Renewable energy sources, including solar and wind power, are becoming increasingly significant in daily life and business [1-2]. In particular, solar energy has been playing a role in each nation's grid electricity. For PV solar energy sources, Maximum Power Point Tracking (MPPT) algorithms are becoming increasingly comprehensive and frequently used [3-5]. The Perturbation and Observation (P&O) method is a famous and efficient conventional MPPT algorithm [6]. To find MPP maximum power working points in the presence of changeable ambient temperature and illumination [7–9], a grid-connected PV solar energy source [10], and a grid-connected PV source with variable load and voltage [11], several articles continue to propose innovative MPPT methods.

In addition to being increasingly efficient and diverse, the proposed MPPT algorithms also include the well-known P&O and INC algorithms [12], back-propagation adaptive MPPT algorithms [13], extreme detection MPPT algorithms (extremum seeking) [14], the geometric MPPT algorithm that combines sliding mode control [15], the neural algorithm [16], the slide mode algorithm [17], and numerous other diverse MPPT algorithms.

Combining the traditional MPPT P&O and INC algorithms with sustainable adaptive control algorithms has recently shown to be a highly fruitful research area. A flexible MPPT P&O method is suggested by Femia et al. [18]. An enhanced MPPT P&O method with a programmable perturbation step is proposed.

The author presents an enhanced MPPT INC method in [19-20], including an adaptive variable perturbation stage. In addition, the fuzzy model and neural model-based intelligent MPPT algorithms successfully preserve PV solar power while operating the MPPT optimally in a changing environment [21–23].

From the above achievements, the paper proposes a new adaptive neuro-fuzzy inference system that integrates fuzzy logic with ANN functionalities. Based on the interrelatedness of the variables, an ANN may train the Surgeon fuzzy controller to generate the exact membership functions for the variables [24, 25].

A comprehensive rule foundation may also be created by deriving the weights of the nodes. The PV array voltage, current, solar irradiance, and surrounding temperature may be utilized as the model's input. In addition, this paper will present the boost converter model by the switching network averaging method. Improve output voltage quality with PI controller-based current controller design.

The article structure includes part 1 of the general introduction. Part 2 introduces the PV solar power source model. Section 3 presents the new adaptive ANFIS-MPPT P&O algorithm. Section 4 gives modelling and control of the Boost converter current. Part 5 presents and analyses the simulation and experimental results of the new ANFIS-MPPT P&O algorithm adapted to MATLAB / Simulink with a 50-W PV system. Finally, the conclusions are presented in section 6.

2. Model of Solar Energy Source PV

The nonlinear equation of V-I characteristics of PV solar energy source, including Ns cells connected in series and N_p cells connected in parallel, has the following form:

$$V_g = -I_g R_s \left(\frac{N_s}{N_p}\right) + \left(\frac{N_s}{A}\right).ln\left\{1 + N_s I_{ph} - \frac{N_s}{N_p I_0}\right\} \qquad (1)$$

Where:
A = q/AKT
q – electric charge
A – completion factor
K – constant Boltzmann
T – absolute temperature

The equivalent circuit of the PV solar cell is shown in Figure 1.

The V-I characteristic depends on the illuminance percentage Kins expressed by the expression:

V_g=-0.9I_g+123,69ln{1,0+123,45(13,45K_ins-I_g)}   (2)

From there, a family of V-I standard curves according to the illuminance of PV solar cells is shown in Figure 2.

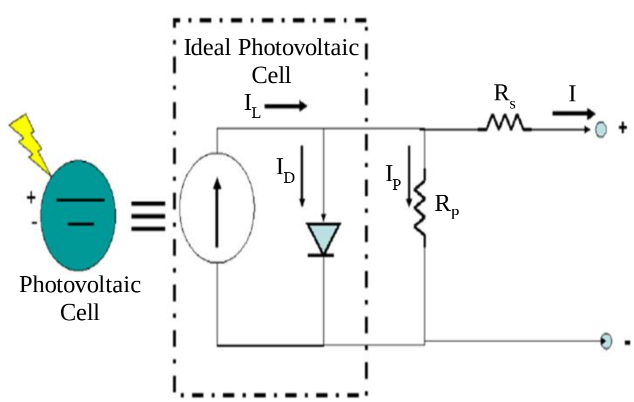

Fig. 1 Equivalent electricity of solar cell source PV

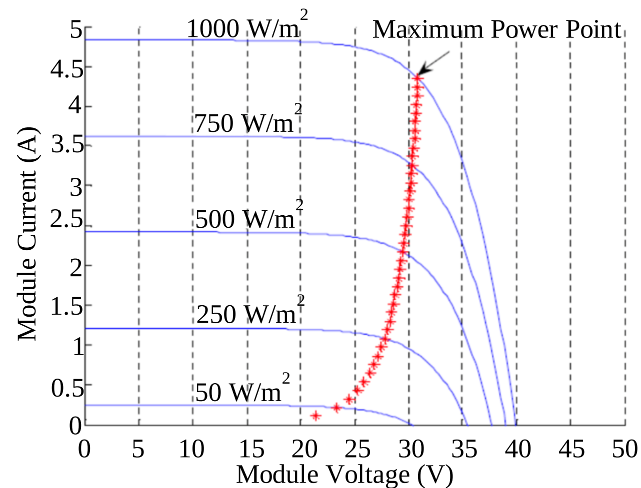

Fig. 2 Standard characteristic curve family V-I according to parameters

3. MPPT P&O Algorithm Combined with ANFIS Control

3.1. MPPT Algorithm P&O

This is the most commonly used MPPT detection algorithm based on voltage perturbation and dP/dt observations. This derivative shows whether the voltage is high or low and needs to decrease or increase until the product is zero. The principle of Maximum Power Point Tracking (MPPT) of the P&O algorithm is shown in Figure 3. The P&Q algorithm diagram is shown in Figure 4.

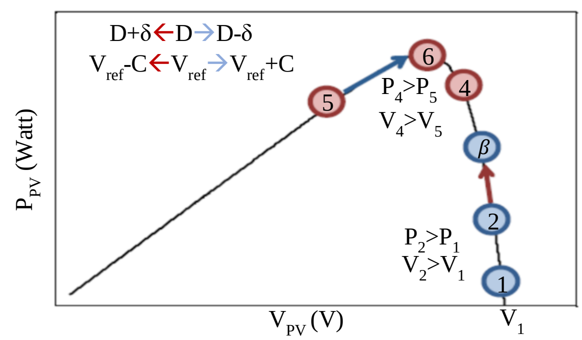

Fig. 3 Principle of Maximum Power Point Tracking (MPPT) of P&O algorithm

A summary of the operating principle of the P&O algorithm is given in Table 1.

Table 1. The operating principle of the P&O algorithm

Case	Noise dV	Change in Power dP	Next Noise
1	dV>0	dP>0	Positive
2	dV>0	dP<0	Minus
3	dV<0	dP>0	Minus
4	dV<0	dP<0	Positive

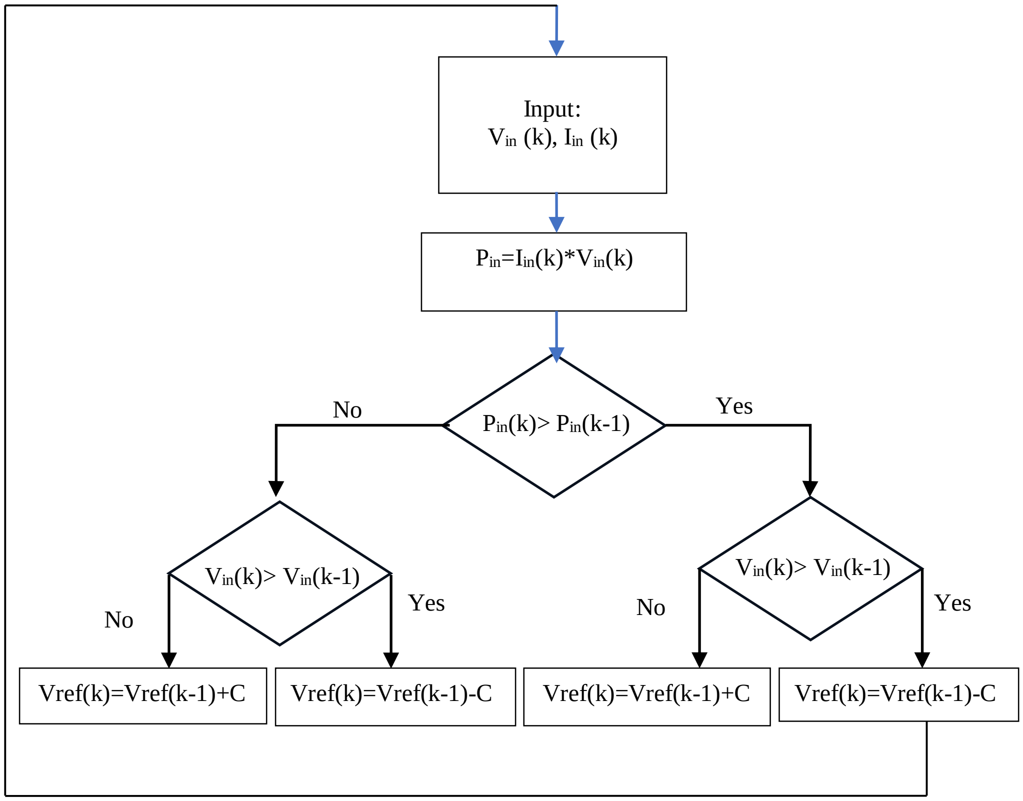

Fig. 4 shows the output power of PV as a function of current

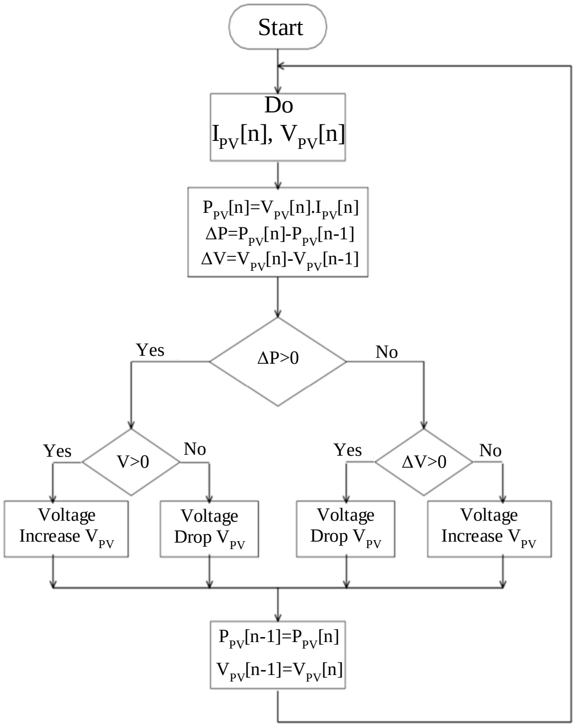

Fig. 5 Control diagram of the P&O algorithm

The 4th case of Table 1 shows that the output power is reduced by reducing the operating voltage, so the next noise step must be positive, which means the voltage needs to be increased. The detailed control diagram of the P&O algorithm is shown in Figure 5. Figure 5 shows that at the beginning of the cycle of the P&O method, two sensors are used to measure the output current and voltage of the PV photovoltaic source. From there, calculate instantaneous power Pn=Un.In. Then, compare the immediate power value Pn with the previous value Pn-1. If the power Pn= Pn-1, update the matter immediately and terminate the process. The algorithm increases voltage if the power and voltage difference between two consecutive cycles is positive. Otherwise, it decreases voltage. Conversely, if the voltage and power difference between two successive cycles is negative, the algorithm improves the voltage or decreases the operating voltage. The process is repeated until the maximum power is obtained.

3.2. The Proposed ANFIS Algorithm

The architecture of the ANFIS with two inputs (x, y) and one output (z) is given in Figure 6.

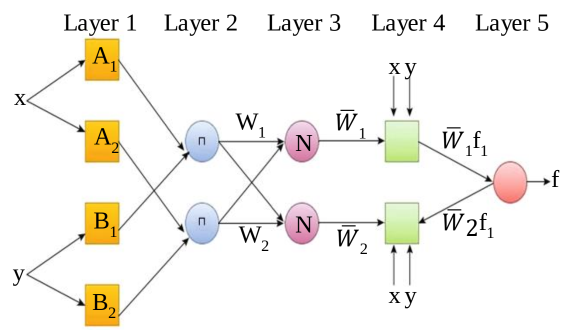

(a)

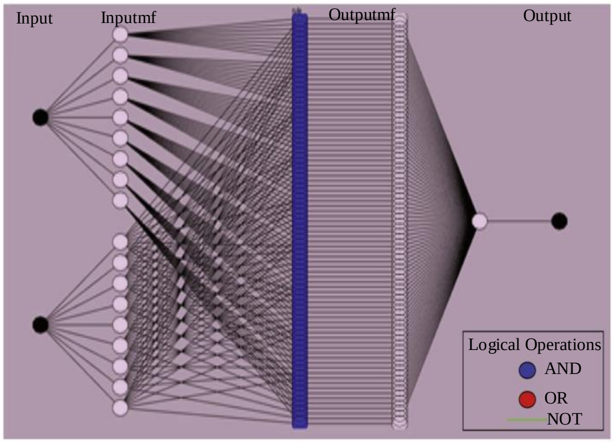

(b)
Fig. 6 Architecture of an ANFIS

Layer 1: Every node is typically flexible. Node I in this layer O1 relies on the input of the corresponding node I membership functions for its output.

$$O_{1.}i = \mu_{AI}(x), \text{for } i = 1,2 \quad (3)$$

$$O_{1.}i = \mu_{BI-2}(y), \text{for } i=3,4$$

Here, the inputs are x and y, and the corresponding Ai and B_i sets are fuzzy sets in the parametric form. The membership functions for this study's inputs, *x* and *y*, are Gaussian.

Layer 2: It has fixed nodes, and the node i's output represents the outcome of its input functions. This layer, referred to as a neural network layer, multiplies information.

$$O_{2.}i = \omega_i = \mu_{Ai}(x) * \mu_{B\,i}(y), \text{for } i=1,2 \quad (4)$$

Layer 3: Every node is fixed and identified by N. O_3, the total of the firing strengths of the rules from layer two is referred to as the "standardized firing strengths" in the output of layer 3.

$$O_{3.}i = \overline{\omega_i} = \frac{\omega_i}{\omega_1+\omega_2}, \text{for } i=1,2 \quad (5)$$

Layer 4: The nodes' features may be changed, and the parameters follow suit. This fuzzy logic node has pi, qi, and RI parameter values. In Equation (6), the node's output is shown.

$$O_{4,i}i = \overline{\omega_i}f_i = \overline{\omega_i}(p_i, x + p_i, y + r_i), \text{for } i=1,2 \quad (6)$$

Layer 5: It has a single fixed node, and the sum of all incoming signals is combined to produce its output. Equation (7) depicts the node's output function.

$$O_{5.}i = \overline{\omega_i}f_i = \frac{\sum_i \omega_i f_i}{\sum_i \omega_i}, \text{for } i=1,2 \quad (7)$$

4. Boost Converters

4.1. Modelling the Boost Variable with the Closed Network Average Method

The method of averaging the switching network is of interest today because the obtained model is close to the physical model, which can describe the loss-causing elements such as resistance when conducting current through the valve, voltage drop on valves, and some parasitic electrical circuits.

The purpose of the method is to replace the part of the circuit with the switching element with a two-door network. Then, the nonlinear switching network is replaced with a linear network through averaging.

In the diagram Boost converter Figure 7, the switching network includes valve MOSFET and diode. Because the input current to port 1 $i_1(t)$ is the current through the inductor, it can be considered an independent variable; the output voltage on the capacitor $v_2(t)$ is the voltage on the load that changes only when the load changes, so also consider is the independent variable. Therefore, voltage $v_1(t)$ and $i_2(t)$ are considered as dependent variables, as shown in Figure 7.

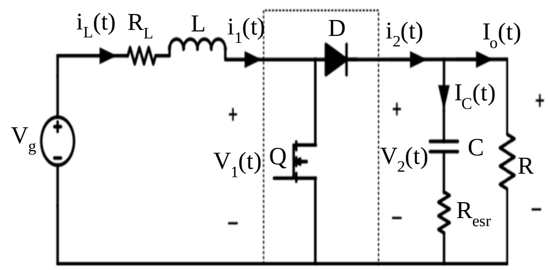

Fig. 7 The switching circuit in the diagram boosts the converter

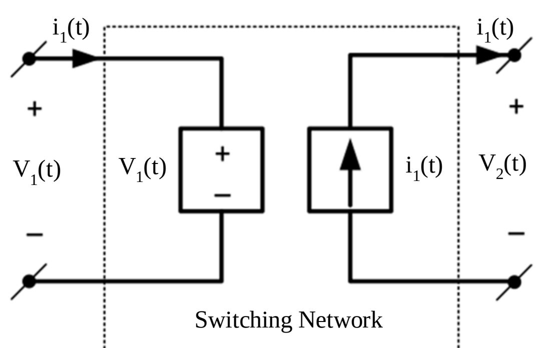

Fig. 8 Switched network model

Their waveforms are shown in Figure 8 according to the operation analysis of the Boost converter diagram. Average voltage $v_1(t)$ and current $i_2(t)$ over a period T_s assuming $v_2(t)$ and i1(t) pulses are negligible or vary almost linearly:

$$(V_1(t))_{T_s} = (1 - d(t))(V_2(t))_{T_s} = d'(t)(V_2(t))_{T_s} \quad (8)$$

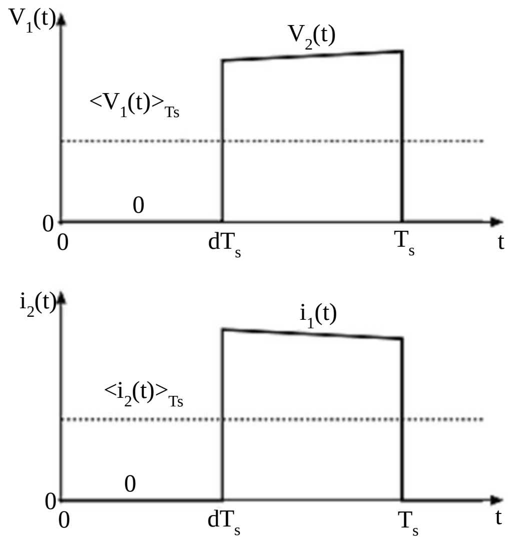

Fig. 9 Voltage form V1(t) on MOSFET and current form $i_2(t)$ through diode

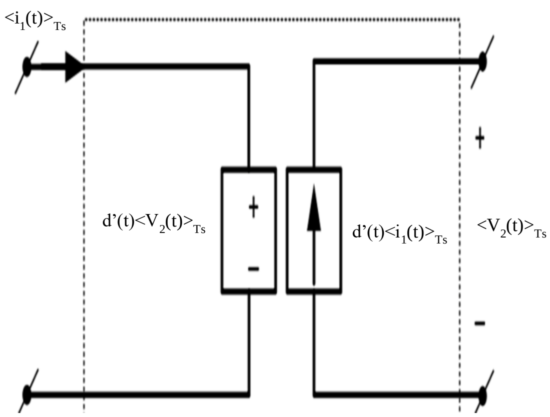

Fig. 10 Average model

$$\langle i_1(t)\rangle_{T_s} = (1-d(t))\langle i_1(t)\rangle_{T_s} = d'(t)\langle i_2(t)\rangle_{T_s} \tag{9}$$

Proceed to linearize the model in Figure 10 by introducing small fluctuations:

$$\begin{pmatrix} V_g(t) = V_g + \widehat{V_g}(t) \\ i_L(t) = I_L + \widehat{\iota_L(t)} \\ V_1(t) = V_1 + \widehat{V_1(t)} \\ i_2(t) = I_2 + \widehat{\iota_2}(t) \\ V_2(t) = V_2 + \widehat{V_2}(t) \\ d = D' + \widehat{d\,(t)} \\ d' = 1 - d = D' + \widehat{d\,(t)} \end{pmatrix} \tag{10}$$

The dependent voltage source at input port 1 becomes:

$$\begin{aligned}\langle V_1(t)\rangle = d'(t)\langle V_2(t)\rangle &= \left(D' - \hat{d}(t)\right)\left(V_2 + \widehat{V_2}(t)\right) \\ &\approx D'\left(V_2 + \widehat{V_2}(t)\right) - V_2\hat{d}(t)\end{aligned} \tag{11}$$

First term $D'\left(V_2 + \widehat{V_2}(t)\right)$ shows the dependence on the output voltage $\left(V_2 + \widehat{V_2}(t)\right)$ in proportion D', described by the dependent voltage source. Rank $V_2\hat{d}(t)$ is the source controlled by the modulation factor $\hat{d}(t)$ and should become an independent voltage source connected in series in the circuit. The dependent current is shown:

$$\begin{aligned}\langle i_2(t)\rangle = d'(t)\langle i_1(t)\rangle &= \left(D' - \hat{d}(t)\right)\left(I_1 + \widehat{I_1}(t)\right) \\ &\approx D'\left(I_1 + \widehat{\iota_1}(t)\right) - I_1\hat{d}(t)\end{aligned} \tag{12}$$

Rank $D'\left(I_1 + \widehat{\iota_1}(t)\right)$ express dependence on $\left(I_1 + \widehat{\iota_1}(t)\right)$ in proportion D' should be described by the dependent current source. Rank $I_1\hat{d}(t)$ is the current source controlled by the factor $\hat{d}(t)$ and becomes an independent current source in parallel with the circuit. From there, the average model of the switching network for the boost circuit. From the above analysis, the average model for the Boost converter is shown:

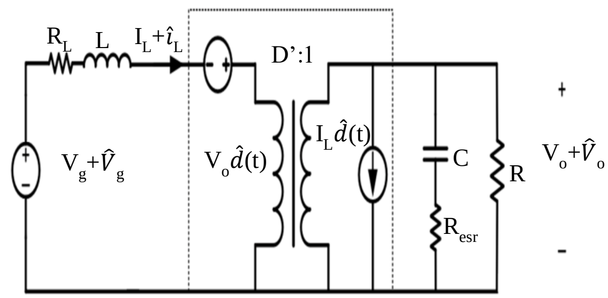

Fig. 11 Average model for Boost circuit

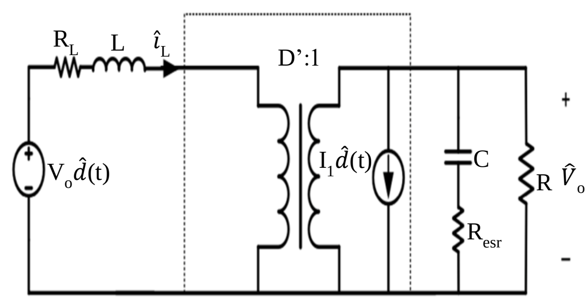

Fig. 12 Small signal average model for Boost circuit when $\widehat{v_g} = 0$

Considering the small signal model, as shown in Figure 12, it is necessary to determine the important transfer functions for the design of the current controller:

$$\begin{cases} G_{VD} = \dfrac{\widehat{v_0}}{\hat{d}}\Big|\,\widehat{v_g} = 0 \\ G_{id} = \dfrac{\widehat{\iota_L}}{\hat{d}}\Big|\,\widehat{v_g} = 0 \end{cases} \tag{13}$$

To find these transfer functions, we remove the influence of the source $\widehat{v_g} = 0$ in the model Figure 11 and 12 to obtain a simple model:

Next, convert to the transformer's primary, Laplace the circuit, and then, based on the circuit calculation, derive the desired transfer function G_{vd} and G_{id}.

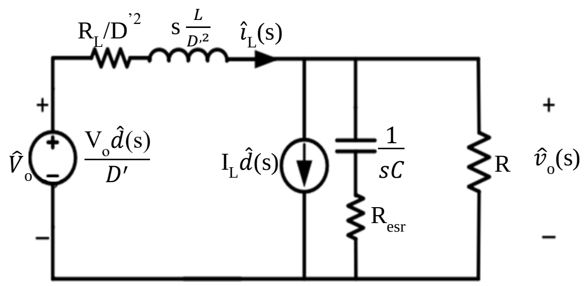

Fig. 13 Laplace of the converter circuit

The voltage balance in the circuit shown in Figure 13 is obtained:

$$G_{vd}(s)=\frac{\widehat{V_0}(s)}{\hat{d}(s)}$$
$$=\frac{V_0}{D'}\frac{\left(1-\frac{R_L+sL}{RD'^2}\right)(1+sR_{esr}C)}{s^2\frac{LC(R+R_{esr})}{RD'^2}+s\left(\frac{R_L(R+R_{esr})C+L}{RD'^2}+R_{esr}C\right)+\frac{R_L}{RD'^2}+1} \tag{14}$$

The current balance in the circuit shown in Figure 13 is obtained:

$$\hat{\imath}_L(s)=\frac{1}{D'}\left[I_L\hat{d}(s)+\frac{s(R+R_{esr})C+1}{(1+sR_{esr}C)R}\hat{v}_0(s)\right] \tag{15}$$

Combined with $\hat{v}_0$t from the transfer function, the transfer function of the current object can be deduced:

$$G_{id}(s)=\frac{\hat{\imath}_L(s)}{\hat{d}(s)}$$
$$=\frac{V_0}{RD'^2}\frac{s(R+2R_{esr})C+2}{s^2\frac{LC(R+R_{esr})}{RD'^2}+s\left(\frac{R_L(R+R_{esr})C+L}{RD'^2}+R_{esr}C\right)+\frac{R_L}{RD'^2}+1} \tag{16}$$

4.2. Design of Current Controller

The diagram of the control current.

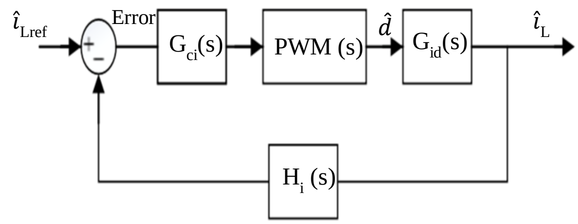

Fig. 14 The diagram of the control current

The current control loop has fast dynamic characteristics, and the voltage loop has lower dynamic features. As a result, the inductor current can vary very quickly compared to the output voltage. According to Equation (16), the transfer function of the current control loop:

$$G_{id}(s)=\frac{0{,}008347s+48}{1{,}739.10^{-8}.s^2+7{,}658.10^{-5}s+4{,}07} \tag{17}$$

5. Results and Discussion

The MATLAB simulations of a structure fuzzy logic-based MPPT controller and a Boost converter are built, as shown in Figure 15.

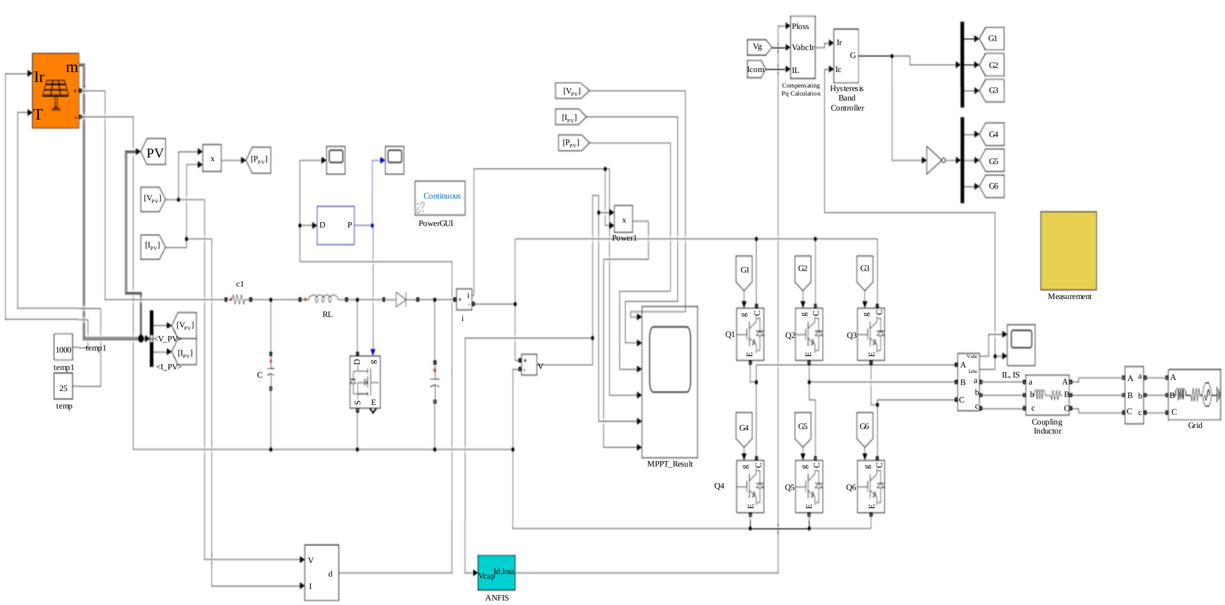

Fig. 15 The structure of FL based MPPT controller and a boost converter

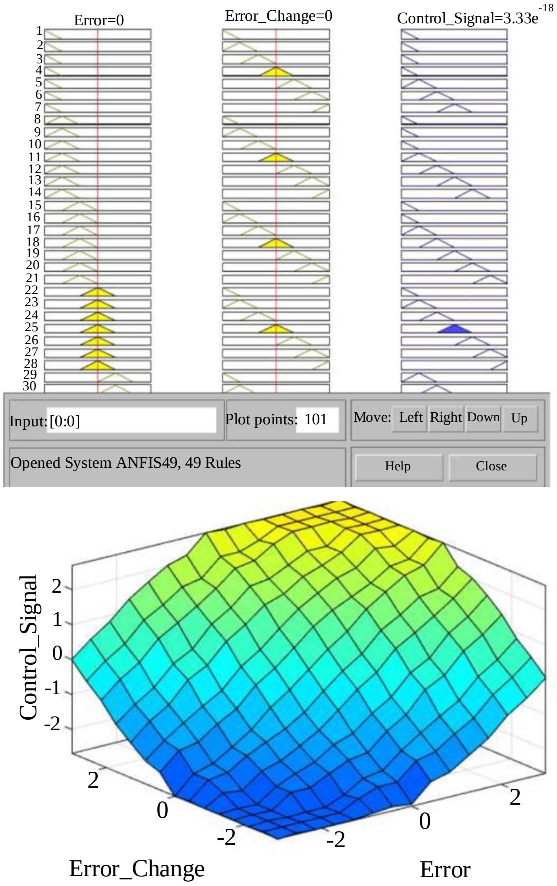

Fig. 16 The surface view of the FL model

The surface view of the FL model is expressed in Figure 16. The fuzzy rules for two inputs and output are shown in Figure 17.

Power rating input from the user	= 2.00kW
Minimum number of panels required per string	= 8
Maximum number of panels connected per string without reaching maximum voltage	= 10
The minimum power rating of the solar PV plant	= 1.80 kW
Maximum power possible per string without reaching maximum DC voltage	= 2.25 kW
Actual number of panels per string	= 9
Number of strings connected in parallel	= 1
Actual solar PV plant power	= 2.03 kW

Selected parameters of the boost converter are shown in Table 2. Three phases' currents are shown in Figure 18. Irradiance is 1000 W/m2, and the temperature kept constant at 25°C is shown in Figure 19. The input voltage, current, and power for the PV system are shown in Figure 20. The output voltage, current, and power for the PV system are shown in Figure 21.

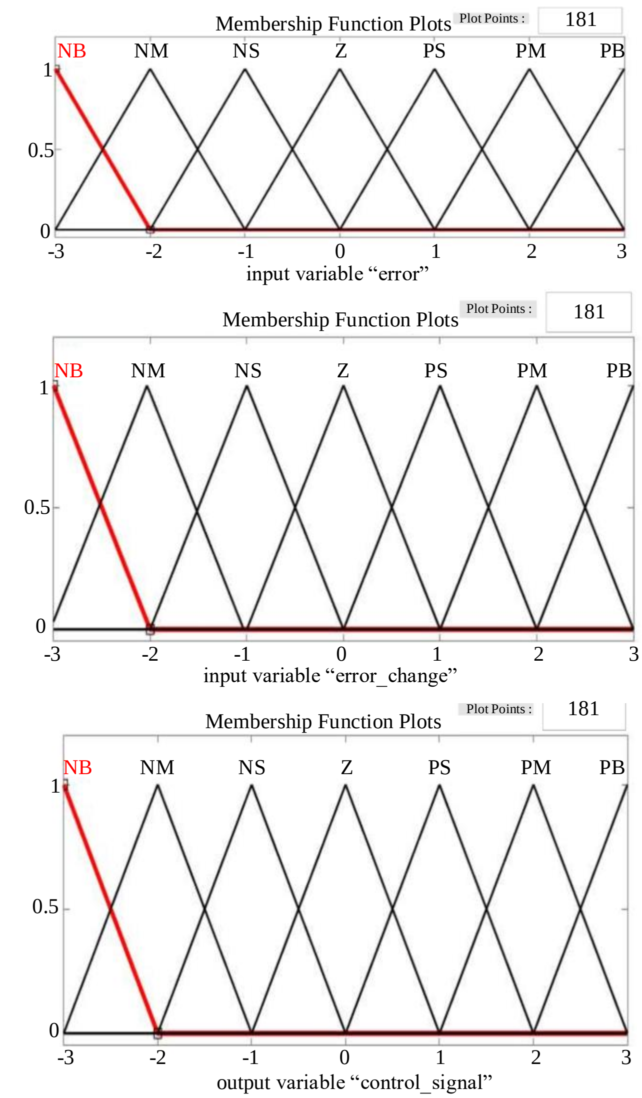

Fig. 17 The fuzzy rule for two inputs and an output

Table 2. Selected parameters of the boost converter

Parameter	Value
Input Voltage	98V
Input current	140A
Duty ratio	0.35
Inductor	4mH
Load resistance	12 Ω
Output capacitor	89µF
Input capacitor	4500 µF
Switching frequency	20kHz

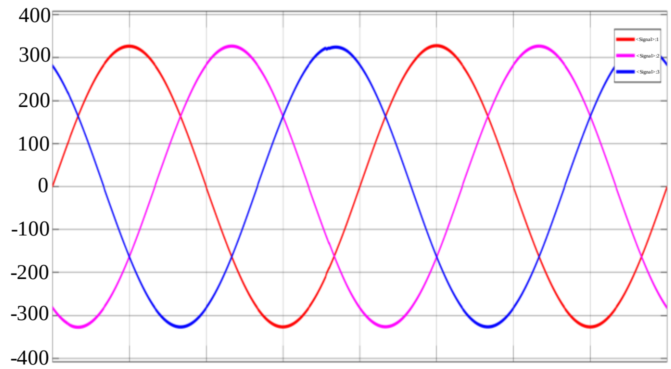

Fig. 18 Three phases' currents

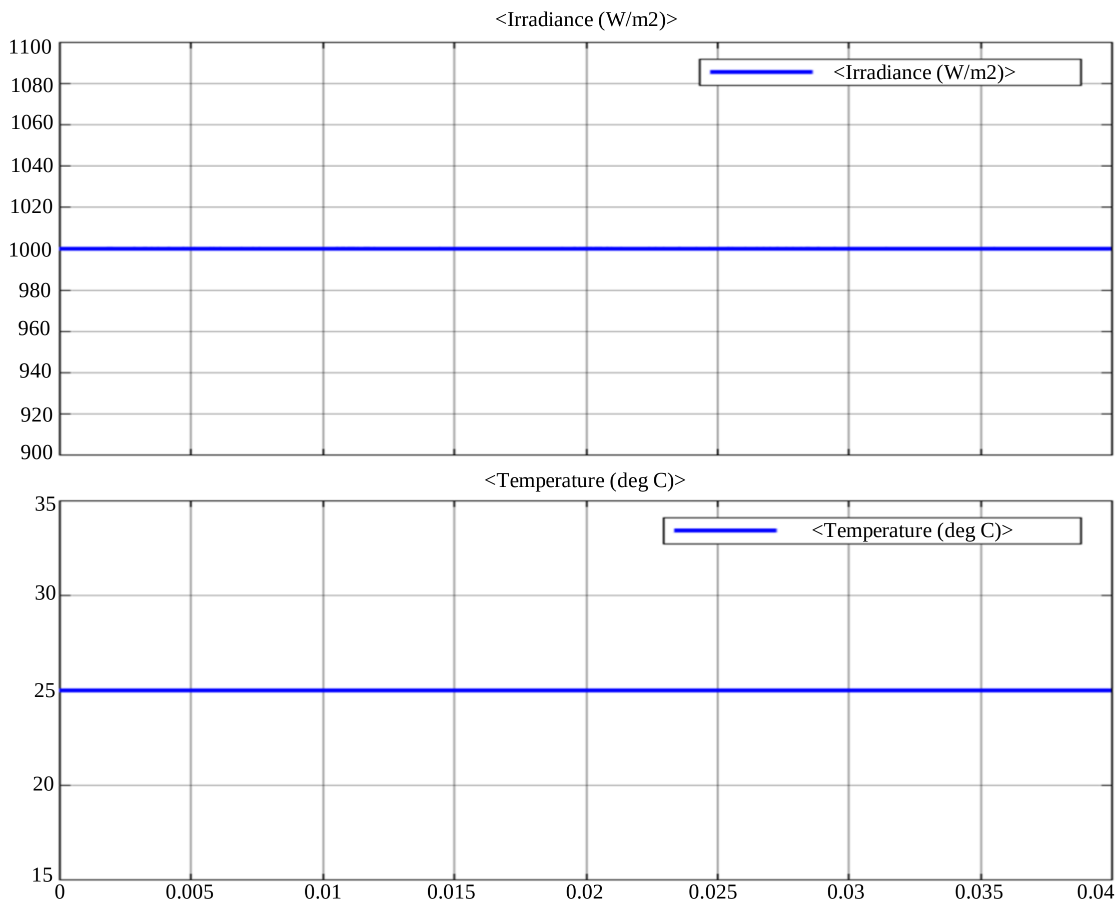

Fig. 19 Irradiance is 1000 W/m2, and the temperature kept constant at 25°C

Based on the modeling above findings, the suggested MPPT controller is modeled at STC (1000 W/m2 and 25 °C) (Figures 18, 19, 20, and 21). After a delay of 10 ms, the PV power output climbs abruptly from zero to about the ANFIS-MPPT P&O (500 W). Since the MPPT controller constantly forces the PV module to function at the ANFIS - MPPT P&O, the power output for the system with the ANFIS - MPPT P&O controller settles at MPP. Without the controller, the PV power input for the system decreases and stabilizes at around 3.5kW.

The input voltage to the PV system is around 350V, and the input current is about 140A. The boost converter's PV power production starts to decline at around 500 W. This is because the internal resistance of the module does not match the load resistance. The PV input current and sinusoidal three-phase current are about 600A, and the input voltage is around 100V. This demonstrates how effectively and effectively the ANFIS -MPPT P&O controller operates.

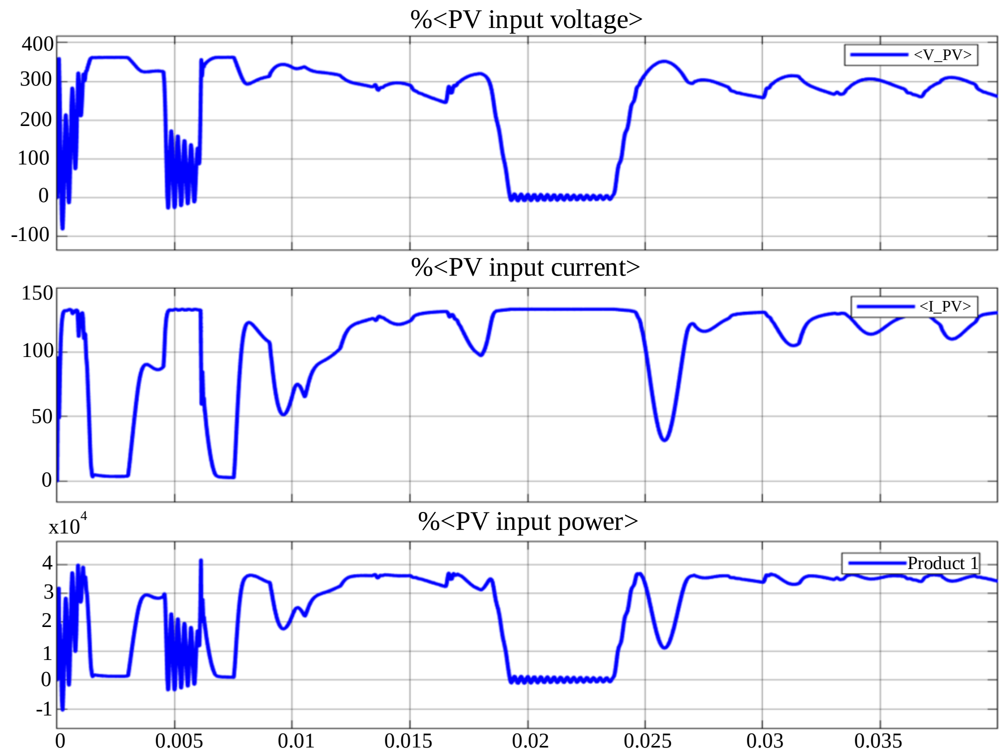

Fig. 20 The input voltage, current, and power for PV system

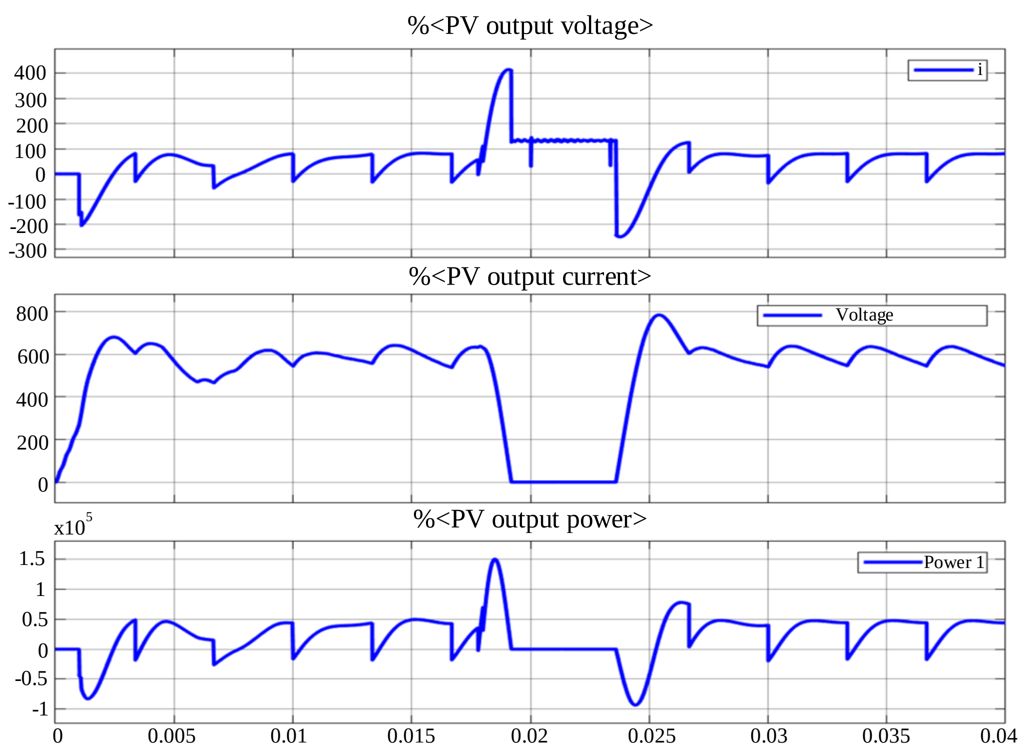

Fig. 21 The output voltage, current, and power for PV system

6. Conclusion

This study gave the suggested ANFIS-based MPPT controller's design, modeling, and assessment. The real-time MPP of the solar module was closely monitored to understand the maximum power output that a PV module is capable of producing under a particular set of solar irradiation and temperature. The components and subsystems of the proposed MPPT controller were modeled and simulated in the MATLAB/SIMULINK environment. According to simulation findings, the suggested ANFIS-based MPPT can consistently and efficiently monitor the maximum power point of PV modules under various weather circumstances. The boost converter's control signal was created using the suggested ANFIS power controller, producing good MPPT results. The approach's effectiveness will be shown by applying the research results to real devices in the future and contrasting them with alternative control methods.

Acknowledgments

This project study was supported by all researchers and funding from the University of Transport and Communications and the University of Economics-Technology for Industries.

References

[1] Phebe Asantewaa Owusu, and Samuel Asumadu-Sarkodie, "A Review of Renewable Energy Sources, Sustainability Issues and Climate Change Mitigation," *Cogent Engineering*, vol. 3, no. 1, pp. 1-14, 2016. [CrossRef] [Google Scholar] [Publisher Link]

[2] Renewables Account for Almost Three Quarters of New Capacity in 2019, IRENA, 2020. [Online]. Available: https://www.irena.org/News/pressreleases/2020/Apr/Renewables-Account-for-Almost-Three-Quarters-of-New-Capacity-in-2019#:~:text=Renewables%20accounted%20for%20at%20least,cent%20of%20net%20additions%20respectively

[3] Mohammad Hossein Ahmadi et al., "Solar Power Technology for Electricity Generation: A Critical Review," *Energy Science and Engineering*, vol. 6, no. 5, pp. 340-361, 2018. [CrossRef] [Google Scholar] [Publisher Link]

[4] Mariusz Malinowski, Jose I. Leon, and Haitham Abu-Rub, "Solar Photovoltaic and Thermal Energy Systems: Current Technology and Future Trends," *Proceedings of the IEEE*, vol. 105, no. 11, pp. 1-15, 2017. [CrossRef] [Google Scholar] [Publisher Link]

[5] Apel Mahmud, and Jahangir Hossain, *Renewable Energy Integration: Challenges and Solutions*, Springer Science and Business Media, New York, pp. 1-447, 2014. [Google Scholar] [Publisher Link]

[6] Mihnea Rosu-Hamzescu, and Sergiu Oprea, "Practical Guide to Implementing Solar Panel MPPT Algorithms," *Microchip Technology Inc.*, vol. 58, pp. 1-16, 2013. [Google Scholar] [Publisher Link]

[7] Cherukuri Santhan Kumar, and Rayapudi Srinivasa Rao, "A Novel Global MPP Tracking of Photovoltaic System based on Whale Optimization Algorithm," *International Journal of Renewable Energy Development*, vol. 5, no. 3, pp. 1-8, 2016. [CrossRef] [Google Scholar] [Publisher Link]

[8] Al-Attar Ali Mohamed, Ahmed Lotfy Haridy, and A.M. Hemeida, "The Whale Optimization Algorithm based Controller for PMSG Wind Energy Generation System," *Proceedings of the 2019 International Conference on Innovative Trends in Computer Engineering (ITCE)*, pp. 438-443, 2019. [CrossRef] [Google Scholar] [Publisher Link]

[9] Kok Soon Tey et al., "Improved Differential Evolution-Based MPPT Algorithm Using SEPIC for PV Systems Under Partial Shading Conditions and Load Variation," *IEEE Transactions on Industrial Informatics*, vol. 14, no. 10, pp. 4322-4333, 2018. [CrossRef] [Google Scholar] [Publisher Link]

[10] Ke Guo et al., "An Improved Gray Wolf Optimizer MPPT Algorithm for PV System with BFBIC Converter Under Partial Shading," *IEEE Access*, vol. 8, pp. 103476-103490, 2020. [CrossRef] [Google Scholar] [Publisher Link]

[11] Bhubaneswari Parida, S. Iniyan, and Ranko Goic, "A Review of Solar Photovoltaic Technologies," *Renewable and Sustainable Energy Reviews*, vol. 15, no. 3, pp. 1625-1636, 2011. [CrossRef] [Google Scholar] [Publisher Link]

[12] Trishan Esram, and Patrick L. Chapman, "Comparison of Photovoltaic Array Maximum Power Point Tracking Techniques," *IEEE Transactions on Energy Conversion*, vol. 22, no. 2, pp. 439-449, 2007. [CrossRef] [Google Scholar] [Publisher Link]

[13] Vicente Salas et al., "Review of the Maximum Power Point Tracking Algorithms for Stand-Alone Photovoltaic Systems," *Solar Energy Materials and Solar Cells*, vol. 90, no. 11, pp. 1555-1578, 2006. [CrossRef] [Google Scholar] [Publisher Link]

[14] Nicola Femia et al., *Power Electronics and Control Techniques for Maximum Energy Harvesting in Photovoltaic Systems*, CRC Press, pp. 1-366, 2012. [Google Scholar] [Publisher Link]

[15] D.P. Hohm, and M.E. Ropp, "Comparative Study of Maximum Power Point Tracking Algorithms," *Progress in Photovoltaics: Research and Applications*, vol. 11, no. 1, pp. 47-62, 2003. [CrossRef] [Google Scholar] [Publisher Link]

[16] Dezso Sera et al., "On the Perturb-and-Observe and Incremental Conductance MPPT Methods for PV Systems," *IEEE Journal of Photovoltaics*, vol. 3, no. 3, pp. 1070-1078, 2013. [CrossRef] [Google Scholar] [Publisher Link]

[17] B. Bendib et al., "An Intelligent MPPT Approach Based on Neural-Network Voltage Estimator and Fuzzy Controller, Applied to a Stand-Alone PV System," *2014 IEEE 23rd International Symposium on Industrial Electronics (ISIE)*, pp. 404-409, 2014. [CrossRef] [Google Scholar] [Publisher Link]

[18] Jaw-Kuen Shiau, Yu-Chen Wei, and Bo-Chih Chen, "A Study on the Fuzzy- Logic-Based Solar Power MPPT Algorithms Using Different Fuzzy Input Variables," *Algorithms*, vol. 8, no. 2, pp. 100-127, 2015. [CrossRef] [Google Scholar] [Publisher Link]

[19] Roberto F. Coelho, Filipe M. Concer, and Denizar C. Martins, "Analytical and Experimental Analysis of DC-DC Converters in Photovoltaic Maximum Power Point Tracking Applications," *IECON 2010 - 36th Annual Conference on IEEE Industrial Electronics Society*, pp. 2778-2783, 2010. [CrossRef] [Google Scholar] [Publisher Link]

[20] Roberto F. Coelho, Walbermark M. dos Santos, and Denizar C. Martins, "Influence of Power Converters on PV Maximum Power Point Tracking Efficiency," *2012 10th IEEE/IAS International Conference on Industry Applications*, pp. 1-8, 2012. [CrossRef] [Google Scholar] [Publisher Link]

[21] Robert W. Erickson, and Dragan Maksimovic, *Fundamentals of Power Electronics*, 2nd ed., Springer Science and Business Media, pp. 1-883, 2001. [Google Scholar] [Publisher Link]

[22] W.W. Colonel, and T. McLyman, *Transformer and Inductor Design Handbook*, 3rd ed., CRC Press, pp. 1-667, 2004. [Google Scholar] [Publisher Link]

[23] R. Zaitsu, "Voltage Mode Boost Converter Small Signal Control Loop Analysis Using the TPS61030", *Texas Instruments, Application Report*, pp. 1-21, 2009. [Google Scholar] [Publisher Link]

[24] Hisham Hussein, Ali Aloui, and Badr AlShammari, "ANFIS-Based PI Controller for Maximum Power Point Tracking in PV Systems," *International Journal of Advanced and Applied Sciences*, vol. 5, no. 2, pp. 90-96. 2018. [CrossRef] [Google Scholar] [Publisher Link]

[25] M.A. Abido, M. Sheraz Khalid, and Muhammed Y. Worku, "An Efficient ANFIS-Based PI Controller for Maximum Power Point Tracking of PV Systems," *Arabian Journal for Science and Engineering*, vol. 40, no. 9, pp. 2641–2651, 2015. [CrossRef] [Google Scholar] [Publisher Link]